

Chapter 2: Multi-wavelength observations of solar flares

Solar extreme ultraviolet (EUV) flare observations and findings from the Solar Dynamics Observatory (SDO) EUV Variability Experiment (EVE)

Thomas N. Woods, Francis G. Eparvier and James P. Mason

Laboratory for Atmospheric and Space Physics, University of Colorado, 3665 Discovery Drive, Boulder, CO 80303, USA

email: tom.woods@lasp.colorado.edu, frank.eparvier@colorado.edu,
james.mason@lasp.colorado.edu

Abstract. New solar soft X-ray (SXR) and extreme ultraviolet (EUV) irradiance observations from NASA Solar Dynamics Observatory (SDO) EUV Variability Experiment (EVE) provide full coverage from 0.1 to 106 nm and continuously at a cadence of 10 seconds for spectra at 0.1 nm resolution. These observations during flares can usually be decomposed into four distinct characteristics: impulsive phase, gradual phase, coronal dimming, and EUV late phase. Over 6000 flares have been observed during the SDO mission; some flares show all four phases, and some only show the gradual phase. The focus is on the newer results about the EUV late phase and coronal dimming and its relationship to coronal mass ejections (CMEs). These EVE flare measurements are based on observing the sun-as-a-star, so these results could exemplify stellar flares. Of particular interest is that new coronal dimming measurements of stars could be used to estimate mass and velocity of stellar CMEs.

Keywords. Irradiance, solar flares, soft X-ray, extreme ultraviolet

1. Introduction

The NASA Solar Dynamics Observatory (SDO) has three solar instruments on-board to study the radiative output, magnetic field, and variability of the solar plasma with high time cadence. The extreme ultraviolet (EUV) irradiance instrument, named the EUV Variability Experiment (EVE), measures the solar irradiance (full-disk radiation). The solar irradiance is the major energy driver of the Earth's upper atmosphere and is a key variable in understanding a variety of planetary and heliophysical phenomena. Solar irradiance measurements also show the variability of the solar radiation over all time scales ranging from minutes to decades and can provide calibration for some solar physics spectrographs and imagers. The high cadence (10 sec) and modest spectral resolution (0.1 nm) for SDO EVE is also valuable for examining the spectral variations during flare events. While EVE observations provide full-disk spectra, the irradiance variations during many of the flare events have corresponded to flaring in a single active region as confirmed by examining the SDO Atmospheric Imaging Assembly (AIA; Lemen *et al.* 2012) solar EUV images. Therefore, an EVE spectrum minus the pre-flare spectrum provides a flare spectrum over the full EUV range when only one dominant flare event is in progress at a time. The EVE spectra over the full EUV range, EUV images from AIA, and magnetic fields from SDO Helioseismic and Magnetic Imager (HMI) provide a powerful combination to study flare processes.

Solar flares have long been an interest for sudden ionosphere disturbances and their effect on radio communication (e.g., Dellinger 1937), and flare observations have been made

for decades in the visible, primarily in H α (e.g., Ellison 1946), and also in the soft X-ray (SXR) and EUV ranges from sounding rocket and satellite experiments (e.g., Friedman 1963). Hudson (2010, 2011), Doschek & Feldman (2010), Lang (2009), and Aschwanden *et al.* (2009b) provide reviews of recent progress in understanding flares from observations that involve the Solar and Heliospheric Observatory (SOHO), Transition Region and Coronal Explorer (TRACE), Reuven Ramaty High Energy Solar Spectroscopic Imager (RHESSI), Hinode (Solar-B), and Solar TERrestrial RELations Observatory (STEREO) missions. These satellites include imagers in X-ray and EUV broadbands and imaging spectrographs with high spectral resolution but limited EUV range.

The new and exciting aspects of the SDO EVE observations for flare studies are the spectral coverage over the full EUV range from 0.1 to 106 nm with 0.1 nm resolution and the continuous monitoring of the solar activity with high cadence of 10 sec. The EVE flare observations have revealed that many EUV emissions do not behave like the X-ray variations that are often used for classifying the flare magnitude and as a proxy for EUV emissions in models such as the Flare Irradiance Spectral Model (FISM; Chamberlin *et al.* 2008). The EVE flare observations are being used to improve the understanding of flare energetics and their impacts on Earth's space environment.

The new irradiance observations by EVE are significantly improved over the previous solar EUV irradiance instruments flying on SOHO, Thermosphere Ionosphere Mesosphere Energetics Dynamics (TIMED), and Geostationary Operational Environmental Satellite (GOES) spacecraft. The EVE suite includes the Multiple EUV Grating Spectrograph (MEGS) that provides EUV spectral observations with spectral resolution of 0.1 nm from 6 to 105 nm, cadence of 10 sec, and accuracy to better than 20%. The EUV SpectroPhotometer (ESP) provides broadband observations between 0.1 and 39 nm with even higher cadence of 0.25 sec and with improved accuracy of better than 10%. Woods *et al.* (2012) provide an overview of EVE's science plans, instrument design, and data products. Didkovsky *et al.* (2012) provide an overview of the ESP instrument and its calibration, and Hock *et al.* (2012) provide an overview of the MEGS instrument and its calibration. SDO was launched on 2010 February 11, and EVE began normal operations on 2010 May 1.

The flare data from EVE shown here are primarily from the MEGS-A channel measuring the spectrum from 7 to 37 nm and the ESP zeroth-order channel (0.1-7 nm band) as the flare variations are most evident in these wavelengths. The EVE spectral resolution of 0.1 nm is especially significant for the wavelength range from 7 to 27 nm because previously there have only been broadband (~ 10 nm wide) EUV irradiance measurements at these wavelengths. With EVE's improved spectral resolution and continuous observations with 10-sec cadence and in conjunction with AIA EUV images and HMI magnetic fields, we now have a much more accurate knowledge of how the solar EUV irradiance varies during flare events. While not discussed here, the EVE spectra have better than anticipated wavelength stability and Doppler shifts are evident in the EVE spectra, both for the ± 3 km/sec drift over its 24-hour orbit period and during some flare events (Hudson *et al.* 2011).

2. Four major phases for solar flares

Flares are often decomposed into an impulsive phase with significant non-thermal signatures and a gradual (slow) mostly thermal phase that follows the impulsive phase (Donnelly 1976; Hudson 2010, 2011). The rapid release of energy from magnetic reconnection in the corona accelerates electrons and ions during the impulsive phase, which is often dominated by intense Bremsstrahlung radiation in the hard X-ray (HXR) from

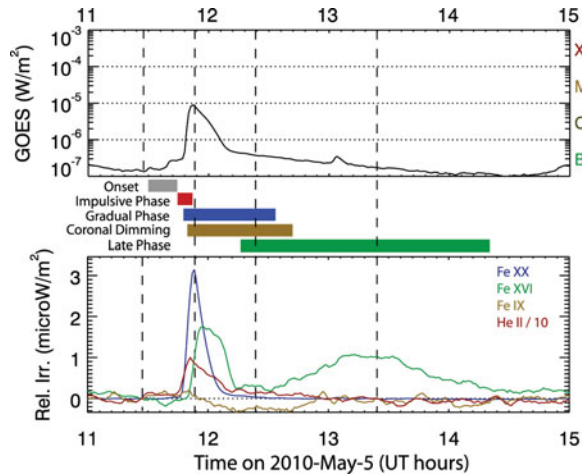


Figure 1. Flare variations for the C8.8 flare on 2010 May 5 as adapted from Woods *et al.* (2011). The relative irradiance (Rel. Irr.), being the solar irradiance spectrum minus the pre-flare spectrum, represents well the flare variations over its different phases. The transition region He II 30.4 nm emission highlights the impulsive phase. We assume that GOES X-ray defines the gradual phase, and the hot corona Fe XX / Fe XXIII 13.3 nm emission behaves almost identically as the X-ray. The cool corona Fe IX 17.1 nm emission is the EUV emission with the largest amount of coronal dimming after the impulsive phase. The warm corona Fe XVI 33.5 nm emission has its first peak a few minutes after the X-ray gradual phase peak and then has a second peak many minutes later. The change in slope of the GOES X-ray during the gradual phase is indicative of the late phase contribution (second Fe XVI peak). The four vertical dashed lines, left to right, are for spectra in Figure 2 of the pre-flare, main phase, coronal dimming, and EUV late phase.

the energetic electrons as they interact with the dense, cool plasma in the solar chromosphere and transition region. These energetic particles heat the chromosphere, and the evaporated plasma rises into the corona during the gradual phase while emitting much of its radiation in the soft X-rays (SXR) and EUV range. This is part of an overall process of cooling the hot plasma in progressively higher post-flare loops that are an indication of magnetic reconnection (e.g., Kopp & Pneuman 1976; Svestka 1989; Raftery *et al.* 2009). The gradual component normally peaks a few minutes after the impulsive phase, and its intensity rise can often be approximated as the time integral of the impulsive component, referred to as the Neupert effect (Neupert 1968). The magnetic reconnection process can be fast, so some flare models have many flaring loops, or strands within such coronal loops, heated at slightly different times to form a continuous source (Warren & Doschek 2005).

Although EVE measures the full-disk irradiance in the extreme ultraviolet (EUV: 100–1100Å) and the soft X-ray (SXR: 1–100Å), flare events can be studied in detail as long as only one major flare is happening at a time, which happens to be most of the time. Woods *et al.* (2011) provide examples of the four major phases seen during flares with the EVE data. These phases include the impulsive phase best seen in transition region emissions such as He II 304Å, gradual phase seen in hot coronal emissions such as the Fe XX/Fe XXIII 133Å, coronal dimming seen in cool corona emissions such as Fe IX 171Å and EUV late phase (ELP), which has a second, broad peak one to five hours after the main flare phases and seen best in the Fe XVI 335Å emission. The X-ray flare classification by the Geostationary Operational Environmental Satellite X-Ray Sensor (GOES/XRS) is identification of the gradual phase, and the derivative of its 1–8Å SXR

emission can be a proxy for the impulsive phase, as related to the Neupert effect (Neupert 1968). The coronal dimming and EUV late phase effects are only observable in the EUV emissions.

Each flare can have its own unique behavior; some flares have all four of these phases, and some flares only have the gradual phase (by definition from the X-ray flare identification by GOES/XRS). For more detailed information, Hudson (2011) reviews flare processes and phases, and Hock *et al.* (2012) identifies different categories of flares based on the new SDO/EVE and SDO/AIA observations of hundreds of flares. Notably the eruptive flares tend to have impulsive phase, gradual phase, and coronal dimming, and some eruptive flares also have the EUV late phase as explained in Section 3. From examining the dozens of EUV emission lines in the EVE spectra during flare events, there are four primary aspects of the flares that dominate the EUV time series: (1) (HXR) impulsive phase, (2) (SXR/EUV) gradual phase, (3) EUV coronal dimming often associated with CME, and (4) EUV late phase that will be explained later in Section 3. Because the EVE flare selection process first starts with identifying flares in the GOES X-ray time series, all of the EVE-identified flares have the gradual phase component. The other EUV flare components are not always present, but these components are more common for eruptive flares. The C8.8 flare on 2010 May 5 is a good example when all four components clearly exist as shown in Figure 1. The various EUV emissions have one or more of these aspects in their time series, and the four emissions that best highlight each component are included in this figure. The EUV spectral variations during this C8.8 flare are shown in Figure 2.

The He II 30.4 nm emission is from the transition region, and it contributes more energy than any other single emission in the EUV range during a flare (see Figure 2B). If the flare has a strong impulsive phase, then the He II emission has a peak a few minutes before the X-ray peak and sometimes a second peak soon after the X-ray peak corresponding to post-flare loop reconnections. This emission sometimes does not exhibit an impulsive phase contribution and just has enhancements during the post-flare loop reconnections. Based on the timing of the He II peak, 55% of the flares in our sample had a strong impulsive phase. The impulsive phase is critical for a myriad of space weather applications because of its indication of the start of the flare event and the possibility of highly energetic radiation and particles that can be created during the impulsive phase. The energetic radiation can include the non-thermal Bremsstrahlung radiation (HXR) and sometimes gamma rays that reach Earth in 8 minutes. Furthermore, the brighter flares are sometimes associated with solar energetic proton (SEP) events that reach Earth in a few hours and coronal mass ejection (CME) events that reach Earth in a couple days.

The Fe XX / Fe XXIII 13.3 nm emission represents the hot corona at 10 to 16 MK, and this emission behaves very similar to the GOES X-ray time series and represents well the flare's gradual phase. This emission is an excellent proxy for the SXR and vice-versa. The gradual phase is characterized as the chromospheric evaporation resulting from the initial heating caused during the impulsive phase. The intense increase in SXR and EUV radiation in the 0.1 to 15 nm range during the gradual phase, as shown in Figure 2B, is important for space weather applications as they are energetic enough to quickly enhance the ionization in Earth's upper atmosphere (80-300 km). Furthermore, the gradual phase typically lasts for many minutes to even hours and thus impacts Earth's atmosphere for a longer period of time than the impulsive phase.

A third EUV emission included in Figure 1 is the Fe IX 17.1 nm emission that represents the cool corona at 0.7 MK. If there is coronal dimming, then the Fe IX through Fe XII emissions usually show coronal dimming as discussed more in Section 4. For this example

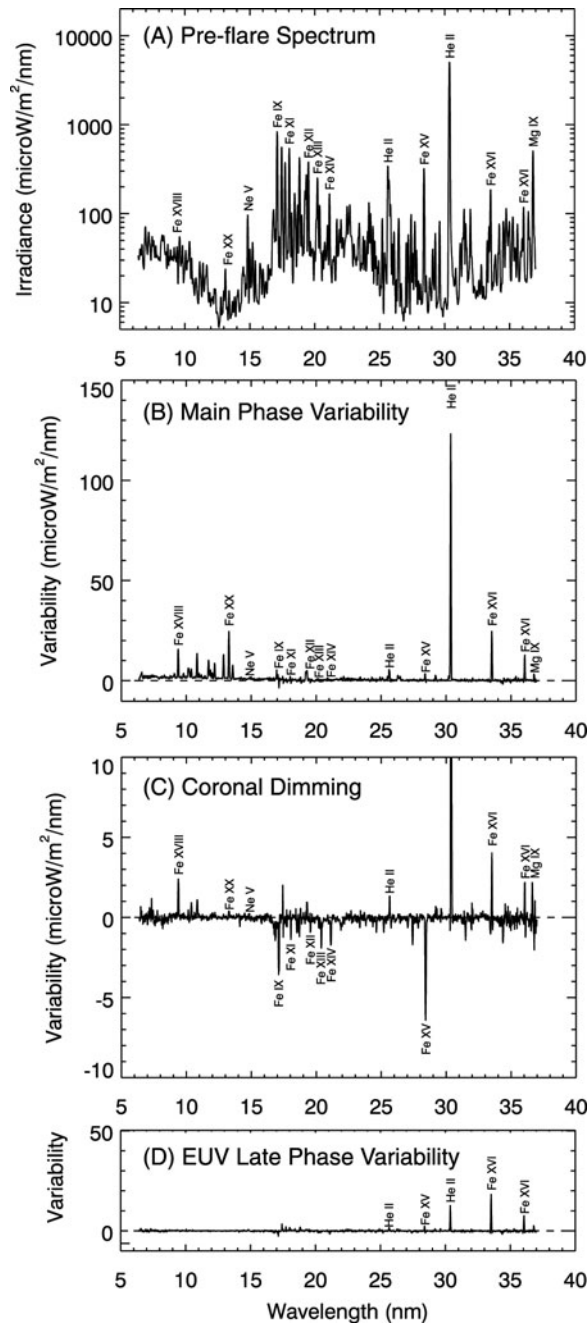


Figure 2. Flare spectral variations from the EVE MEGS A channel (6–37 nm) for the C8.8 flare on 2010 May 5 as adapted from Woods *et al.* (2011). Panel (A) shows the pre-flare spectrum. Panels (B–D) show the variability between the pre-flare irradiance and the main phase, coronal dimming, and EUV late phase, respectively. These results used 5-minute averages taken at the times indicated in Figure 1 as vertical dashed lines.

flare in Figure 1, the Fe IX emission has a large decrease as shown in Figure 2C. The decrease of the Fe IX coronal emission starts near the peak of the impulsive phase, and this emission usually reaches its minimum after the peak of the Fe XX / Fe XXIII emission and sometimes not until after the first peak of the Fe XVI 33.5 nm emission, as is the case in Figure 1. The duration of the coronal dimming can be a few hours to a day or so (Rust 1983; Sterling & Hudson 1997; Reinard & Biesecker 2008). The Fe IX emission showed coronal dimming for 22% of the flares analyzed. The importance of the coronal dimming to space weather is that it is highly correlated with coronal mass ejection (CME) events (e.g., Rust 1983; McIntosh *et al.* 2007). This is indeed the case for these Fe IX coronal dimmings as compared to CMEs detected by coronagraphs aboard SOHO and STEREO (CME lists at <http://sidc.oma.be/cactus/>). Aschwanden *et al.* (2009a) have shown that the amount of coronal dimming can be used to derive CME characteristics such as its mass, so the near real-time EVE Fe IX 17.1 nm data have potential application for providing alerts of CME events.

The warm corona emission in Figure 1 is the Fe XVI 33.5 nm emission that represents a coronal temperature of about 3 MK. Being cooler than the Fe XX, the Fe XVI emission peaks, on average, 6 minutes after the Fe XX and GOES X-ray peak, and this time delay indicates the cooling rate of the post-flare coronal loops in the volume involved in the impulsive and gradual phases. For long duration events (LDEs), the delay for the Fe XVI gradual phase peak is even longer, ranging up to 2 hours for the C3.4 flare on 2010 November 3 (X-ray peak at 13:08 UT). For the 2010 August 1 LDE (C3.2 flare), the delay for the Fe XVI gradual phase peak was 101 minutes. The Fe XV and Fe XVI emissions are also interesting as it sometimes has a second peak, and its irradiance during the second peak is often similar in magnitude as the first peak. This second peak of the Fe XVI (and also Fe XV) emissions occurred about 20% of the time. When there is a second peak, the second peak occurred between 16 and 295 minutes after the first peak during the gradual phase, with an average delay of 75 minutes. In addition, the ratio of the second peak to the first peak ranged from 0.2 to 4.1; the average ratio is 1.2. The importance of these second peaks to space weather is just now being studied in ionosphere-thermosphere models, but it is clear that they contribute to ionization in Earth's atmosphere for even longer than its first peak during the gradual phase. The following Section 3 discusses the importance of this second peak that we refer to as the EUV late phase.

There are dozens of other emission lines in the EUV spectra with several being blends for EVE's 0.1 nm spectral resolution, but these four emission lines selected for Figure 1 represent reasonably well how the other EUV emission lines behave. In particular, the cool coronal Fe IX, Fe X, and Fe XI emissions vary similarly, and the warm coronal Fe XV and Fe XVI emissions have similar variations. The moderately warm coronal Fe XII, Fe XIII, and Fe XIV emissions vary about the same as each other and have the character of coronal dimming similar to the Fe IX emission. Both the much cooler transition region emissions such as the He II 30.4 nm (~ 0.08 MK) and hot coronal emissions Fe XX / Fe XXIII 13.3 nm (10-16 MK) emissions, shown in Figure 1, exhibit their largest increases during the flare's main phase, as do the X-ray measurements, but no significant variations after the flare main phase.

The GOES X-ray emission is also included in Figure 1 as it has sometimes been used as a proxy for the short-term variations of the solar EUV irradiance (e.g., Chamberlin *et al.* 2008). We note that the GOES X-ray emission correlates well with the very hot coronal emissions and that the time derivative of the GOES X-rays (Neupert effect) correlates reasonably well with the transition region emissions. But the GOES X-ray emission in either form does not correlate well with the variations seen in the other coronal emission

lines ($\sim 0.7 - 5$ MK), so additional studies for how to best model these coronal emissions during flares are needed for space weather applications.

3. EUV late phase flares

As defined by Woods *et al.* (2011), the identification of EUV late phase includes:

- i) a second peak of the warm coronal emissions (Fe XV and Fe XVI) several minutes to a few hours after the GOES X-ray peak,
- ii) no significant enhancements of the GOES X-ray or hot coronal emissions (e.g., the Fe XX / Fe XXIII 133Å) during this second peak,
- iii) eruptive event as seen in the AIA images and is also seen as coronal dimming in the Fe IX 171Å emission, and
- iv) a second set of longer loops being reconnected higher than the original flaring loops and at a much later time than the first set of post-flare loops formed just minutes after the flare, as observed in AIA images.

Woods *et al.* (2011) provide an overview of about 200 flares observed during the first year of the SDO mission (May 2010 - April 2011). Of those flares, 88.5%, 11%, and 0.5% of them were C-, M-, and X-class flares, respectively. All of them had a gradual phase (as expected since flare identification starts with finding GOES X-ray peaks), 55% had an impulsive phase, 22% had coronal dimming, and 14% had an EUV late phase. In general, there is higher probability for having impulsive phase, coronal dimming (eruptive), and EUV late phase for the larger flares. For the EUV late phase flares, the disturbance of the coronal loops by the eruption is at about the same time, but the relaxation and cooling down of the heated coronal loops during the post-flare reconnections have different time scales with the longer, upper loops being significantly delayed from the lower loops (Woods *et al.* 2011). The difference in these cooling time scales is related to the difference between the two peak times of the warm coronal emission and is also apparent in the decay profile of the X-ray emissions having two distinct decays, with the first decay slope being steeper (faster) and the delayed decay slope being smaller (slower) during the time of the warm coronal emission second peak. The frequency and relationship of the EUV late phase decay times between the Fe XVI 335Å two flare peaks and X-ray decay slopes are examined by Woods (2014) for all of the EUV late phase flares during the first three years of the SDO mission, and the X-ray dual decay character is exploited to estimate the frequency of EUV late phase flares during the past four solar cycles. The Woods (2014) results indicate that the frequency of EUV late phase flares peaks before and after each solar cycle minimum as highlighted in Figure 3.

The total number of flares found in the GOES X-ray record per year is shown in panel (A) of Figure 3. This result is from searching the GOES record for flare peaks and thus is regardless if a dual-decay X-ray flare is found or not. This plot clearly shows that more flares appear during solar cycle maximum than during minimum, as expected; however, the long-term trend from maximum to maximum is interesting in showing a decrease in the number of flares since 1990. That is, the number of flares during Solar Cycle 23 maximum in 2000-2003 is lower than the flares during Cycle 22 maximum in 1989-1992. This decrease is seen for all levels (C, M, and X) and the decrease for X-class flares is larger than the M-class flares, which in turn has a decrease larger than the C-class flares. Furthermore, the number of flares during Cycle 24 maximum in 2011-2013 is even more reduced as compared to Cycle 23 maximum. Of course, the Solar Cycle 24 maximum period is not necessarily over yet, but many of the solar proxies, such as sunspot number and 10.7-cm radio flux (F10.7), appear to have already had their peak for this cycle in late 2011. This downward trend for flares during cycle maximum is also seen in the

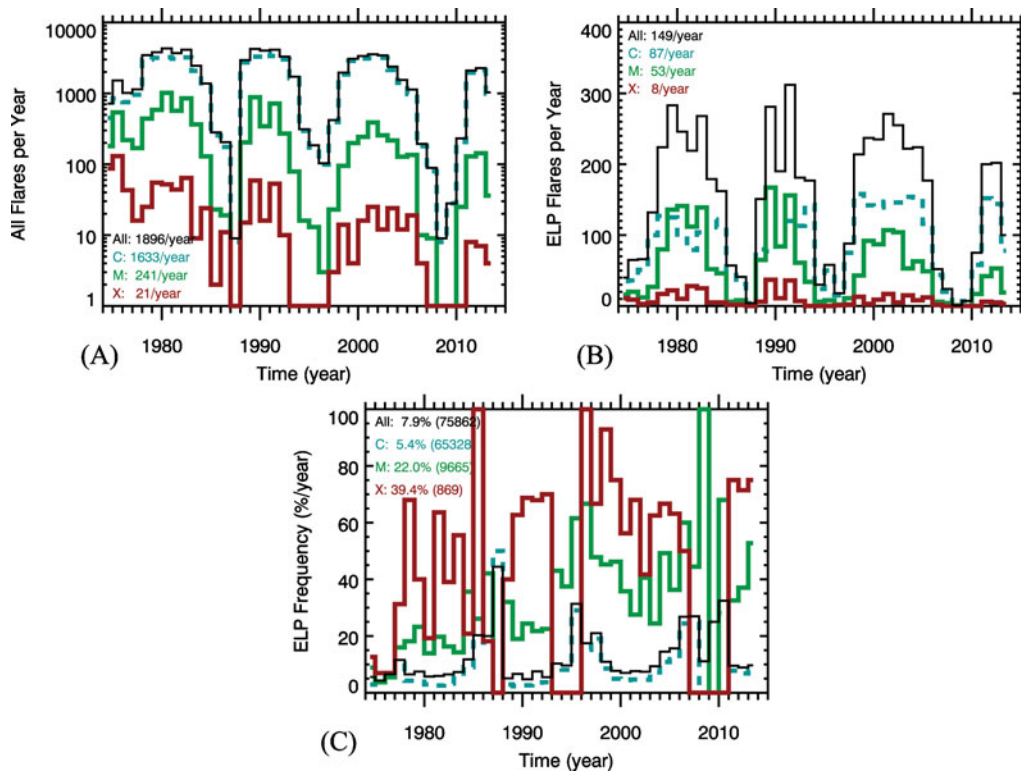


Figure 3. Annual Variations of Potential EUV Late Phase (ELP) Flares as adapted from Woods (2014). The dual-decay algorithm results are compiled into annual averages for C-, M-, and X-class flares separately. Panel (A) shows the number of all flares identified per year in the GOES X-ray data. Panel (B) shows the number of potential ELP flares identified per year. The solar cycle trend is clear in both panels (A) and (B), and there is an interesting trend that there are fewer flares in sequential cycle maxima since the 1990s. Panel (C) shows the ratio of the number of ELP flares to all flares, and this ratio represents the frequency that flares might be ELP flares. The ELP frequency for all flares and C-class flares has peaks right before and right after solar cycle minimum and is lower during solar cycle maximum. The ELP frequency for M- and X-class flares can be more confusing because there are very few, or no, large flares for years during and nearby solar cycle minimum.

cycle-minimum trend, although the minimum trend is less clear with the number of M and X flares sometimes being close to zero near cycle minimum. The wider than usual cycle minimum in 2007-2010 may also contribute to the trend for the flares during cycle minimum.

One concern with any long-term solar trend is if the performance and calibration of the instruments could be changing enough to influence the observed trend. The series of GOES/XRS instruments have been cross-calibrated with concurrent measurements from multiple GOES satellites, and their calibrations are thought to have an accuracy of at least 30% (private communication, R. Viereck & W. Neupert 2013). Furthermore, we have flown calibration rockets for Thermosphere Ionosphere Mesosphere Energetics and Dynamics/Solar EUV Experiment (TIMED/SEE) and SDO/EVE for the past ten years, and these comparisons to GOES/XRS irradiances have consistently shown differences of less than 30%. The downward trend in number of flares is almost a factor of two for M and X flares from one maximum to the next, so instrumental effects at the 30% level cannot be a major concern for these trend results. Then the logical conclusion is that the

downward trend is due to a long-term decrease in solar activity. Russell *et al.* (2010) and Fröhlich (2011) have reported that solar activity has been decreasing since the 1990s, and these results also support this conclusion.

The results for the dual-decay X-ray (proxy for EUV late phase) flares are shown in panels (B) and (C) of Figure 3. Panel (B) shows the number per year, and bottom panel shows the relative number (percent) relative to the total number of flares per year. These results are considered to be a proxy for ELP flares, but with the understanding that there is about 50% uncertainty in these values and also larger uncertainty during cycle maximum. Panel (B) of number of potential ELP flares follows a similar pattern as the total number of flares in having more events during cycle maximum than during minimum. Panel (C) may be more enlightening because it represents the frequency that flares might be ELP flares. The ELP frequency for all flares and C-class flares have peaks before and after solar cycle minimum of about 20% to 30% and is lower during solar cycle maximum at about 10%. The cycle minima were in 1985, 1995, and 2008. Even with the 50% uncertainty for these results, this result of solar cycle dependence for ELP flare frequency is at least a three- σ result. Furthermore, this behavior is consistently seen for all four solar cycles.

The ELP flare frequency for M and X flares can be more confusing because there are very few, or no, large flares for years during cycle minimum. Ignoring the periods near cycle minima when there are often no X-class flares, the frequency for ELP flares for larger flares is about 50% and is significantly higher than the results for the C-class flares. Many X-class flares are two-ribbon flares or long-duration events (LDEs) and are associated with larger and more complex active regions. The confirmed ELP flares during the SDO mission are associated with the more complex active regions that have multiple sets of coronal loops, so perhaps it is reasonable that M- and X-class flares could have more ELP flares than the C-class flares that often have a single set of coronal loops.

4. Coronal dimming in EVE data

It was a surprise to the EVE team that EVE flare data indicated coronal dimming (decrease in irradiance during flares) for the cooler coronal emission lines. Coronal dimming has been known from solar EUV images since the 1970s (e.g., Rust & Hildner 1976; Rust 1983), but they have not been seen in solar EUV irradiance records until the EVE observations. Studies using the Solar and Heliospheric Observatory (SOHO) Extreme-ultraviolet Imaging Telescope (EIT; Delaboudiniere *et al.* 1995) made clear associations to the source of coronal mass ejections and have established that extreme ultraviolet (EUV) dimmings are a good indicator of the apparent base of the white light CME (Thompson *et al.* 2000; Harrison *et al.* 2003; Zhukov & Auchère 2004). Thus, dimmings are usually interpreted as mass depletions due to the loss or rapid expansion of the overlying corona (Hudson *et al.* 1998; Harrison & Lyons 2000; Zhukov & Auchère 2004). This interpretation is supported by observations of simultaneous and co-spatial dimmings in solar EUV images taken at multiple wavelengths (e.g., Zarro *et al.* 1999; Sterling *et al.* 2000; Harra & Sterling 2001).

Coronal dimming is of particular interest for the space weather community. CMEs, when directed toward Earth, can cause geomagnetic storms. The negative consequences of these storms on our space-based and even ground-based technology are well established (National Research Council 2008); therefore, understanding CMEs and improving predictions for CME properties are important for space weather. We aim to establish parameterizations of coronal dimming and correlate them with CME velocity and mass, two key components of CME geoeffectiveness. These coronal dimming analyses hold little

promise, however, of predicting the southward component of the CME's magnetic field - the third important indicator of CME geoeffectiveness.

Extended studies of coronal dimmings have begun to develop a statistical understanding of these events. Reinard & Biesecker (2008) found that coronal dimmings are more likely to occur near active regions, and typically have a rapid decrease in emission followed by a more gradual recovery, lasting from 3 to 12 hours and rarely persisting longer than one day (whereas true coronal holes tend to persist for many days). Although CMEs are also observed to occur without dimmings, Reinard & Biesecker (2009) found that non-dimming CMEs all have speeds of less than 800 km/s, suggesting a more intimate connection between the CME and dimming properties. Krista & Reinard (2013) found further correlations between dimming magnitudes, flares, and CME mass by studying variations between recurring eruptions and dimmings. Similar observations are now routine with the Solar Dynamics Observatory (SDO; Pesnell *et al.* 2012) Atmospheric Imaging Assembly's (AIA; Lemen *et al.* 2012) seven EUV channels. Additionally, dimming has been observed numerous times in SDO/EVE irradiance measurements.

Various physical processes can lead to similar observational signals, particularly if one is focused on only a single emission line. This is particularly true in the case of EVE data being used independently where no spatial information can be used to differentiate the source of an observed dimming. This shortcoming can be solved by examining multiple emission lines in the EVE spectra and examining SDO AIA images. Mason *et al.* (2014) have identified six processes that can cause dimming as being mass-loss dimming (CME event), thermal evolution, obscuration, wave dimming, Doppler dimming, and bandpass shift. Mason *et al.* (2014) explains each of these processes in more detail and provides a case study for the 7 August 2010 coronal dimming event. For this specific event and several other events, the mass-loss dimming is the dominant processes that cause dimming in the EVE data.

The expectation for mass-loss dimming is that the amount of dimming is proportional to the mass loss and that all corona Fe emissions originating in the CME initiation region (i.e., not the confined, flaring loops) would have the same level of dimming. While this expectation is seen with EUV images at multiple wavelengths, the EVE time series for this 2010 event (and many other events) indicate that the dimming amount decreases with the hotter Fe emissions. While thermal dimming could play a role in such behavior, it is known from the AIA analysis that thermal dimming is not a major contribution for this 7 August 2010 event. Mason *et al.* (2014) identified the difference between EVE and AIA dimming results as related to main (impulsive/gradual) phase effects modifying the full-disk irradiance measurement by EVE, and they developed an analysis technique for the EVE coronal dimming data that effectively corrects for the main phase peak effects in the time series to isolate better the mass-loss dimming contribution.

As an example, the results from this correction are shown in Figure 4 for the 7 August 2010 dimming event (Mason *et al.* 2014). The corrected dimming amount from the EVE data is about 3% for the Fe IX 17.1 nm and Fe XII 19.5 nm and is consistent with the AIA results that are also included in this figure for the core dimming region found in the AIA solar EUV images. As expected (intended), the EVE corrected results are much more self-consistent with each other than the uncorrected results. Our expectation is that the slope could represent the CME speed, and the depth could represent the CME mass. Our analysis of about 30 dimming events confirms these expectations. Mason *et al.* (2015) finds that the CME speed estimate is about 600 km/sec times the dimming slope in units of %/hour and that the CME mass estimate is about 10^{12} kg times the dimming depth in units of % using the coronal dimming results from the Fe IX 17.1 nm emission line.

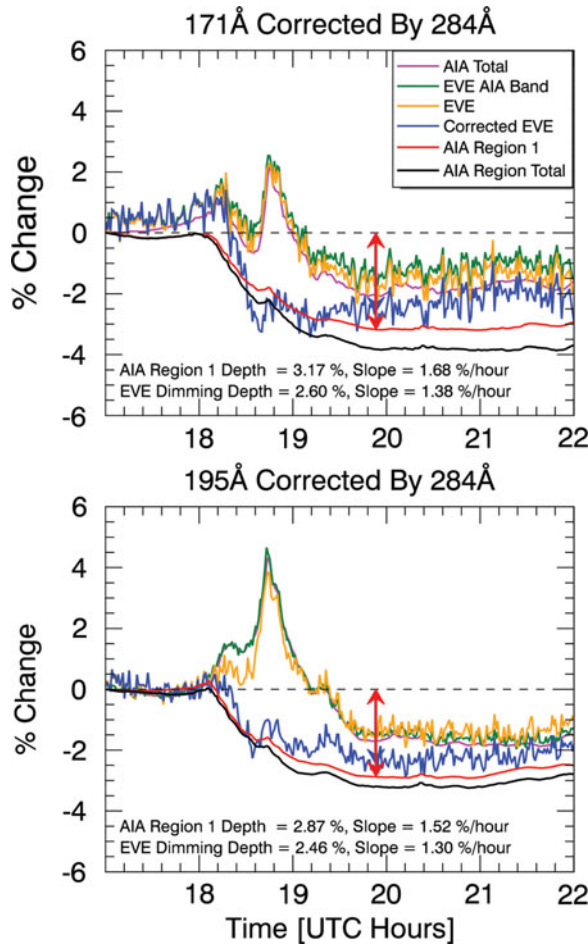


Figure 4. Comparisons of EVE and AIA light curves for coronal dimming as adapted from Mason *et al.* (2014). The EVE raw data show the main phase contributions and less dimming than the AIA dimming results (AIA Region 1 and AIA Region Total). The AIA Total is the AIA signal integrated over the full disk and is in agreement with the EVE raw data. The Corrected EVE data, as corrected for the main phase contribution using the Fe XV 28.4 nm emission time series, indicate very similar level of dimming as the AIA mass-loss dimming component (labeled as AIA Region 1). The estimated CME mass and speed from multi-viewpoint coronagraph measurements is $6.4 \times 10^{12} \pm 5.0 \times 10^{11}$ kg and 850 ± 27 km/sec, respectively.

5. Conclusions

Prior to the SDO mission, the flare irradiance models have been using the GOES X-ray signal as a proxy for the gradual phase and the derivative of the X-ray signal as a proxy for the impulsive phase emissions. It is clear now with the SDO EVE and AIA measurements that at least two additional flare components – (a) coronal dimming for cool coronal emissions and (b) an EUV late phase for warm coronal emissions – are required for modeling the EUV irradiance. While coronal dimming and long duration events like post-flare giant arches have been known for some time, their impact on EUV irradiance is now being clarified with the new SDO observations. The new EVE results are also very important for many space weather applications as deposition of the solar EUV irradiance into Earth’s atmosphere depends on the spectral variability, that is which wavelengths are varying, and on the timing that determines the local (regional) effects

on Earth. For example, the ionospheric F layer is expected to have an additional increase one to five hours after the GOES X-ray peaks for EUV late phase flares. These late phase flares are also significant because they can enhance the total EUV irradiance flare variation by a factor of 40% or more when the EUV late phase contribution is included.

The study of the EUV late phase flares indicates that the frequency of EUV late phase flares peaks before and after each solar cycle minimum and has a minimum frequency of occurrence during cycle maximum. This behavior is consistently seen over four cycles. Many ELP flares were seen in the early part of the SDO mission during the initial rise of Cycle 24, and not as many ELP flares were observed during Cycle 24 maximum. This study suggests that this behavior of ELP flares during the SDO mission is normal behavior over the solar cycle. Another important result from this study is that the number of flares has been decreasing since the 1990s. The downward trend is notably greater for the larger M- and X-class flares, being almost a factor of two decrease per cycle.

These EVE flare measurements are based on observing the sun-as-a-star, so these results can also apply for stellar X-ray and EUV observations. It could be an interesting study to compare stellar flare observations, specifically of sun-like stars, to the EVE flare results to understand if the Sun is displaying typical G2V main-sequence star behavior. Of particular interest from the new coronal dimming results from EVE is that new coronal dimming measurements of stars could be used to more directly estimate the mass and speed of stellar coronal mass ejections, a topic that has previously been studied using hypothetical assumptions based primarily on solar flare magnitude or energy.

Obviously, the new EUV irradiance observations from SDO EVE have huge potentials for expanding our understanding of how different EUV emissions vary during flares and how these variations can cause changes in Earth's ionosphere and thermosphere over many different time scales. While we have made some progress in understanding the EUV late phase solar process and coronal dimming relationship to CME mass loss, the wealth of new data from SDO and other solar observatories over the next several years is expected to lead to even more insightful knowledge of the solar processes throughout the flare time series.

Acknowledgments. This research is supported by NASA contract NAS5-02140 to the University of Colorado. The authors thank the SDO/EVE team for providing the high-quality data used in this study. We also thank Vanessa George for her assistance with this manuscript and Alexander Kosovichev for his help with LaTeX formatting.

References

- Aschwanden, M. J., Nitta, N. V., Wuelser, J.-P., Lemen, J. R., Sandman, A., Vourlidas, A., & Colaninno, R. C. 2009a, First Measurements of the Mass of Coronal Mass Ejections from the EUV Dimming Observed with STEREO EUVI A+B Spacecraft, *ApJ*, 706, 376
- Aschwanden, M. J., Wuelser, J.-P., Nitta, N. V., & Lemen, J. R. 2009b, Solar Flare and CME Observations with STEREO/EUVI, *Solar Phys.*, 256, 3
- Chamberlin, P. C., Woods, T. N., & Eparvier, F. G. 2008, Flare Irradiance Spectral Model (FISM): Flare component algorithms and results, *Space Weather J.*, 6, S05001
- Delaboudiniere, J.-P., Artzner, G. E., Brunaud, J., Gabriel, A. H., Hochedez, J. F., Millier, F., Song, X. Y., Au, B., *et al.* 1995, EIT: Extreme-Ultraviolet Imaging Telescope for the SOHO Mission, *Solar Phys.*, 162, 291
- Dellinger, J. H. 1937, Sudden Disturbances of the Ionosphere, *J. Appl. Phys.*, 8, 732
- Didkovsky, L., Judge, D., Wieman, S., & Woods, T. 2012, EUV SpectroPhotometer (ESP) in Extreme Ultraviolet Variability Experiment (EVE): Algorithms and Calibrations, *Solar Phys.*, 275, doi 10.1007/s11207-009-9485-8
- Donnelly, R. F. 1976, Empirical models of solar flare X ray and EUV emission for use in studying their E and F region effects, *J. Geophys. Res.*, 81, 4745

- Doschek, G. A. & Feldman, U. 2010, Topical Review: The solar UV-x-ray spectrum from 1.5 to 2000Å, *J. Phys. B: At. Mol. Opt. Phys.*, 43, 232001
- Ellison, M. A. 1946, Visual and spectrographic observations of a great solar flare, 1946 July 25, *Mon. Not. Roy. Astron. Soc.*, 106, 500
- Friedman, H. 1963, Ultraviolet and X Rays from the Sun, *Ann. Rev. A&A*, 1, 59
- Fröhlich, C. 2011, A four-component proxy model for total solar irradiance calibrated during solar cycles 21-23, *Contrib. Astron. Obs. Skalnaté Pleso*, 35, 1
- Harra, L. K. & Sterling, A. C. 2001, Material Outflows from Coronal Intensity “Dimming Regions” during Coronal Mass Ejection Onset, *ApJ. Lett.*, 561, 215, doi: 10.1086/324767
- Harrison, R. A. & Lyons, M. 2000, A spectroscopic study of coronal dimming associated with a coronal mass ejection, *A&A*, 358, 1097
- Harrison, R. A., Bryans, P., Simnett, G. M., & Lyons, M. 2003, Coronal dimming and the coronal mass ejection onset, *A&A*, 400, 1071
- Hock, R. A., Chamberlin, P. C., Woods, T. N., Crotser, D., Eparvier, F. G., Furst, M., Woodraska, D. L., & Woods, E. C. 2012, Extreme Ultraviolet Variability Experiment (EVE) Multiple EUV Grating Spectrographs (MEGS): Radiometric Calibrations and Result, *Solar Phys.*, 275, doi 10.1007/s11207-010-9520-9
- Hudson, H. 2010, Observations of solar and stellar eruptions, flares, and jets, in *Heliophysics Space Storms and Radiation: Causes and Effects*, ed. C. J. Schrijver & G. L. Siscoe, Cambridge University Press, Cambridge, pp. 123-158
- Hudson, H. 2011, Global Properties of Solar Flares, *Sp. Sci. Rev.*, 158, 5
- Hudson, H. S., Lemen, J. R., St. Cyr, O. C., Sterling, A. C., & Webb, D. F. 1998, X-ray coronal changes during Halo CMEs, *Geophys. Res. Lett.*, 25, 2481, doi: 10.1029/98GL01303
- Kopp, R. A. & Pneuman, G. W. 1976, Magnetic reconnection in the corona and the loop prominence phenomenon, *Solar Phys.*, 50, 85
- Krista, L. D. & Reinard, A. 2013, Study of the Recurring Dimming Region Detected at AR 11305 Using the Coronal Dimming Tracker (CoDiT), *ApJ*, 762, 91
- Lang, K. R. 2009, *The Sun from Space Astronomy and Astrophysics Library*, Springer-Verlag Berlin Heidelberg, 253
- Lemen, J. R., Title, A. M., Akin, D. J., Boerner, P. F., Chou, C., Drake, J. F., Duncan, D. W., Edwards, C. G., *et al.* 2012, The Atmospheric Imaging Assembly (AIA) on the Solar Dynamics Observatory (SDO), *Solar Phys.*, 275, 17
- Mason, J. P., Woods, T. N., Caspi, A., Thompson, B. J., & Hock, R. A. 2014, Mechanisms and Observations of Coronal Dimming for the 2010 August 7 Event, *ApJ*, 789, 61
- Mason, J. P., Woods, T. N., Webb, D., Thompson, B. J., Colaninno, R. C., & Vourlidas, A. 2016, Relationship of Coronal Dimming Slope and Depth to Coronal Mass Ejection Velocity and Mass, *ApJ*, in review.
- McIntosh, S. W., Leamon, R. J., Davey, A. R., & Wills-Davey, M. J. 2007, The Post-eruptive Evolution of a Coronal Dimming, *ApJ*, 660, 1653
- National Research Council, 2008, *Severe Space Weather Events - Understanding Societal and Economic Impacts*, chair D.N. Baker, The National Academies Press, Washington, DC
- Neupert, W. M. 1968, Comparison of Solar X-Ray Line Emission with Microwave Emission during Flares, *ApJ*, 153, L59
- Pesnell, W. D., Thompson, B. J., & Chamberlin, P. C. 2012, The Solar Dynamics Observatory (SDO), *Solar Phys.*, 275, 3
- Raftery, C. L., Gallagher, P. T., Milligan, R. O., & Klimchuk, J. A. 2009, Multi-wavelength observations and modelling of a canonical solar flare, *A&A*, 494, 1127
- Reinard, A. A. & Biesecker, D. A. 2008, Coronal Mass Ejection-Associated Coronal Dimmings, *ApJ*, 674, 576
- Reinard, A. A. & Biesecker, D. A. 2009, The Relationship between Coronal Dimming and Coronal Mass Ejection Properties, *ApJ*, 705, 914
- Russell, C. T., Luhmann, J. G., & Jian, L. K. 2010, How unprecedented a solar minimum?, *Rev. Geophys.*, 48, RG2004, doi:10.1029/2009RG000316
- Rust, D. M. 1983, Coronal disturbances and their terrestrial effects /Tutorial Lecture, *Space Sci. Rev.*, 34, 21
- Rust, D. M. & Hildner, E. 1976, Expansion of an X-ray coronal arch into the outer corona, *Solar Phys.*, 48, 381

- Sterling, A. C. & Hudson, H. S. 1997, Yohkoh SXT Observations of X-Ray “Dimming” Associated with a Halo Coronal Mass Ejection, *ApJ*, 491, L55
- Sterling, A. C., Hudson, H. S., Thompson, B. J., & Zarro, D. M. 2000, Yohkoh SXT and SOHO EIT Observations of Sigmoid-to-Arcade Evolution of Structures Associated with Halo Coronal Mass Ejections, *ApJ*, 532
- Svestka, Z. 1989, Solar flares - The gradual phase, *Solar Phys.*, 121, 399
- Thompson, B. J., Cliver, E. W., Nitta, N. V., Delannée, C., & Delaboudiniere, J.-P. 2000, Coronal dimmings and energetic CMEs in April-May 1998, *Geophys. Res. Lett.*, 27, 1431
- Warren, H. P. & Doschek, G. A. 2005, Reconciling Hydrodynamic Simulations with Spectroscopic Observations of Solar Flares, *ApJ*, 618, L157
- Woods, T. N., 2014, Extreme Ultraviolet Late-Phase Flares: Before and During the Solar Dynamics Observatory Mission, *Solar Phys.*, doi: 10.1007/s11207-014-0483-0
- Woods, T. N., Eparvier, F. G., Hock, R., Jones, A. R., Woodraska, D., Judge, D., Didkovsky, L., Lean, J., *et al.* 2012, Extreme Ultraviolet Experiment (EVE) on the Solar Dynamics Observatory (SDO): Overview of Science Objectives, Instrument Design, Data Products, and Model Developments, *Solar Phys.*, 275, 115
- Woods, T. N., Hock, R., Eparvier, F., Jones, A. R., Chamberlin, P. C., Klimchuk, J. A., Didkovsky, L., Judge, D., *et al.* 2011, New solar extreme ultraviolet irradiance observations during flares, *ApJ*, 739, 59, doi:10.1088/0004-637X/739/2/59
- Zarro, D. M., Sterling, A. C., Thompson, B. J., Hudson, H. S., & Nitta, N. V. 1999, SOHO EIT Observations of Extreme-Ultraviolet “Dimming” Associated with a Halo Coronal Mass Ejection, *Ap. Lett.*, 520, 139
- Zhukov, A. N. & Auchère, F. 2004, On the nature of EIT waves, EUV dimmings and their link to CMEs, *A&A*, 427, 705